Accepted for publication in the ApJ
Preprint typeset using LaTeX style emulateapj v. 11/10/09

LONG TERM RADIATIVE BEHAVIOR OF SGR 1900+14

Ersin Göğüş[1], Tolga Güver[2], Feryal Özel[2], David Eichler[3], Chryssa Kouveliotou[4]

Accepted for publication in the ApJ

ABSTRACT

The prolific magnetar SGR 1900+14 showed two outbursts in the last decade and has been closely monitored in the X-rays to track the changes in its radiative properties. We use archival *Chandra* and *XMM-Newton* observations of SGR 1900+14 to construct a history of its spectrum and persistent X-ray flux spanning a period of about seven years. We show that the decline of its X-ray flux in these two outburst episodes follows the same trend. The flux begins to decline promptly and rapidly subsequent to the flares, then decreases gradually for about 600 days, at which point it resumes a more rapid decline. Utilizing the high quality spectral data in each epoch, we also study the spectral coevolution of the source with its flux. We find that neither the magnetic field strength nor the magnetospheric properties change over the period spanned by the observations, while the surface temperature as well as the inferred emitting area both decline with time following both outbursts. We also show that the source reached the same minimum flux level in its decline from these two subsequent outbursts, suggesting that this flux level may be its steady quiescent flux.

Subject headings: pulsars: individual (SGR 1900+14) − X-rays: bursts

1. INTRODUCTION

Soft Gamma Repeaters (SGRs) and Anomalous X-ray Pulsars (AXPs) belong to a class of objects called magnetars – neutron stars whose X-ray emission is likely to be powered by the decay of their extremely strong magnetic fields (Duncan & Thompson 1992; Thompson & Duncan 1996; Thompson, Lyutikov & Kulkarni 2002). All seven confirmed SGRs and six out of seven confirmed AXPs[5] have emitted energetic bursts of X-rays/soft gamma rays. Burst active episodes of magnetars last anywhere from few hours to months. During their bursting activity, magnetars also exhibit remarkable temporal and spectral changes in their persistent X-ray output. A detailed description of SGRs and AXPs can be found in Woods & Thompson (2006) and Mereghetti (2008).

In the last seven years, new magnetar candidates have emerged, most prominently through transient outbursts (e.g., XTE J1810−197, Halpern & Gotthelf 2005; CXO J164710.2-455216, Israel et al. 2007; SGR J1833−0832, Göğüş et al. 2010). These sources were too dim to be detected in X-rays during their quiescent phases (usually below our detection sensitivity), but their X-ray fluxes increased by up to few hundred times as they entered their outburst episodes. In addition, known magnetar sources also exhibit variations (triggered by bursting activity) in their persistent flux, although typically not as dramatic as those in the transient systems (e.g., Woods et al. 2004). These high X-ray luminosities were instrumental in probing the outburst mechanism of magnetars (Özel & Güver 2007; Güver et al. 2007; Ng et al. 2010). In contrast, the low but persistent flux level of most magnetars requires long term (5-10 years) monitoring to understand (burst-induced) changes in their emission properties (Dib, Kaspi, & Gavriil 2009).

SGR 1900+14 has been one of the most prolific SGRs: it was discovered in 1979 (Mazets, Golenetskij & Guryan 1979), and was detected in a bursting mode again in 1992 (Kouveliotou et al. 1993). In May 1998 the source entered a major outburst episode that lasted about eight months and included the giant flare on 1998 August 27 (Hurley et al. 1999). ASCA and RXTE observations prior to and during the 1998 activation led to the discovery of its 5.16 s spin period (Hurley et al. 1999), its spin-down rate of $\sim 10^{-11}$ s/s and magnetic field of $2 - 8 \times 10^{14}$ G (Kouveliotou et al. 1999), and thus to the confirmation of its magnetar nature. The source resumed a high level of activity in April 2001 (Guidorzi et al. 2001; Kouveliotou et al. 2001) and again in March 2006 (Vetere et al. 2006). As its burst active phases are well separated from each other, SGR 1900+14 is an excellent source to investigate radiative changes both during bursting behavior as well as in burst quiescence.

The first major enhancement in the persistent X-ray flux of SGR 1900+14 was observed at the onset of the 1998 August 27 giant flare: the flux increased by a factor of ∼700 with respect to its level before the activation (Woods et al. 2001). A detailed spectral analysis of the (much longer) flux decay period was not possible due to the lack of continuous monitoring observations with imaging instruments during the decay phase. Esposito et al. (2007) analyzed nine pointed BeppoSAX observations of SGR 1900+14 spanning about five years from May 1997 to April 2002 and noted that the (2−10 keV) flux measured in the last pointing faded significantly with respect to earlier observations. Following the April 2001 activation, the *Chandra* X-ray Observatory and *XMM-Newton* observed SGR 1900+14 at numerous occasions, establishing a valuable dataset for understand-

[1] Sabancı University, Faculty of Engineering and Natural Sciences, Orhanlı-Tuzla, Istanbul 34956, Turkey
[2] Department of Astronomy and Steward Observatory, University of Arizona, 933 N. Cherry Ave, Tucson, AZ, 85721, USA
[3] Department of Physics, Ben-Gurion University of the Negev, Beer-Sheva 84105, Israel
[4] Space Science Office, VP62, NASA/Marshall Space Flight Center, Huntsville, AL 35812, USA
[6] An online catalog of general properties of SGRs and AXPs can be found at http://www.physics.mcgill.ca/∼pulsar/magnetar/main.html

ing the long term behavior of this source in, particular, and of magnetars, in general.

In this paper, we make use of all archival *Chandra* and *XMM-Newton* observations to construct the persistent X-ray flux temporal and spectral history of SGR 1900+14 spanning about seven years following the April 2001 activation. In the next section we introduce the *Chandra* and *XMM-Newton* observations used in this study. In Section 3, we present the results of the spectral analysis and show that the magnetic field strength and the magnetospheric properties remain stable over the period spanned by the observations, while the surface temperature and the inferred emitting area both decline with time following both outbursts. We also show that the source flux shows the same trend in its decline from outburst in both episodes and ultimately reaches the same minimum flux in both cases. We discuss the implications of these results in Section 4.

2. OBSERVATIONS AND DATA ANALYSIS

Between 2001 April 22 and 2008 April 8, SGR 1900+14 was observed 13 times with *Chandra* and *XMM-Newton*Table 1 lists the log of these pointed X-ray observations. We describe below the details of our data reduction.

9

TABLE 1
Log of SGR 1900+14 Observations

Observatory	Observation ID	Observation Date	Exposure Time (ks)
Chandra	2458	2001 Apr 22	20.1
Chandra	2459	2001 Apr 30	18.8
Chandra	3858	2002 Nov 6	48.0
Chandra	3862	2003 Feb 18	25.1
Chandra	3863	2003 Jun 2	25.6
Chandra	3864	2003 Oct 18	25.3
XMM-Newton	0305580101	2005 Sep 20	20.2
XMM-Newton	0305580201	2005 Sep 22	18.7
Chandra	6709	2006 Mar 29	40.0
XMM-Newton	0410580101	2006 Apr 1	13.4
Chandra	7593	2007 Jun 24	12.2
Chandra	8215	2007 Nov 21	12.6
XMM-Newton	0506430101	2008 Apr 8	18.7

2.1. *Chandra*

There are a total of nine *Chandra* observations performed between 2001 April 22 and 2007 November 21. These were all performed using the Advanced CCD Imaging Spectrometer (ACIS) in continuous clocking (CC) mode. We selected rectangular source regions centered at the position of SGR 1900+14 with dimensions $8'' \times 2''$. Our background regions were selected with similar rectangular sizes from source-free regions on the collapsed CC mode image. We calibrated the *Chandra* observations using the CIAO version 4.2 and the CALDB version 4.2.

We extracted the X-ray spectra following the standard *Chandra* data analysis threads with the psextract tool. We then used the mkacisrmf and mkarf tools to create the detector and ancillary response files, respectively. Finally, we re-binned the spectra such that each energy bin would contain at least 50 counts, to decrease the formal errors.

2.2. *XMM-Newton*

We analyzed the X-ray data obtained with the EPIC-pn detector between 2005 September 20 and 2008 April 8. In all observations, the EPIC-pn was operating in full frame mode. The calibration of the data was performed with the Science Analysis Software (SAS) version 9.0.0 and the latest available calibration files as of February 2010, using the task epproc.

We extracted the X-ray source spectra by accumulating events from a circular region with a radius of $32''$ centered at SGR 1900+14. The background regions were selected on the same chip from source free regions with a typical radius of $50''$. We then used the rmfgen and arfgen tools of SAS to generate detector and ancillary response files and re-binned the X-ray spectra such that each energy bin contained at least 50 counts.

3. SPECTRAL ANALYSIS AND RESULTS

We used XSPEC v12.5.1n (Arnaud 1996) to analyze all spectra. We assumed a gravitational redshift correction of 0.306, corresponding to a neutron star mass of 1.4 $M_{\odot}$ and a radius of 10 km. We performed the fits in the 0.8−6.5 keV range, where the lower energy bound is set by the source flux and the higher energy limit is determined by the non-thermal hard X-ray component (Götz et al. 2006) affecting the soft X-ray spectra.

We fit the X-ray spectra using the Surface Thermal Emission and Magnetospheric Scattering (STEMS; Güver, Özel and Lyutikov 2006) model. STEMS is based on the radiative equilibrium atmosphere calculations presented in Özel (2001, 2003) but also includes the effects of magnetospheric scattering on the photons emitted from the neutron star surface as calculated by Lyutikov & Gavriil (2006). The model parameters consist of the surface magnetic field strength, B, surface temperature, T, the magnetospheric scattering optical depth, τ, and the velocity of the particles in the magnetosphere, $\beta = v/c$, where c is the speed of light.

We first fit all 13 spectra simultaneously using STEMS and taking into account the effect of interstellar absorption. We allowed the spectral parameters of all spectra to vary individually. While we did not specify its value a priori, we forced the hydrogen column density to be the same between observations. We found that the magnetic field strength, the scattering optical depth, and the average particle velocity did not vary significantly between different observations. We measured a hydrogen column density of $(2.36 \pm 0.05) \times 10^{22}$ cm^{-2}, assuming solar abundances (Anders & Grevesse 1989). We, therefore, performed all further STEMS fits fixing the hydrogen column density at the above value and forcing the parameters B, τ, and β to be constant between different observations. We still allowed the temperature and the model normalization to vary individually for all spectra. We obtained good fits to all 13 spectra, with a χ^2/dof $= 2370/2438$. In this combined fit, we found a magnetic field strength of $B = (5.0 \pm 0.3) \times 10^{14}$ G, a scattering optical depth of $\tau = 8.7 \pm 0.9$ and a particle velocity of $\beta = 0.37 \pm 0.01$. Below, we discuss the time evolution of the temperature T and the source flux based on these

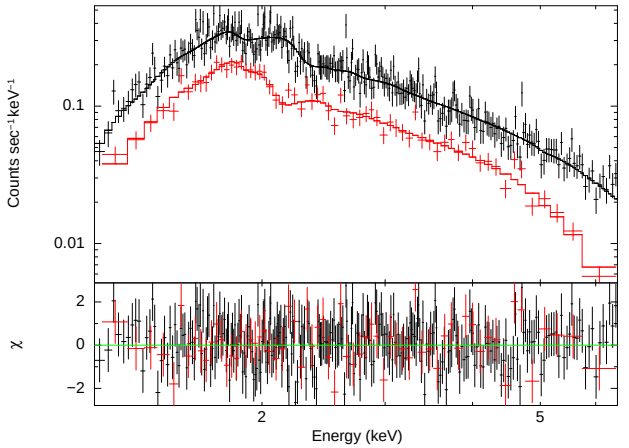

FIG. 1.— Upper panel: two X-ray spectra of SGR 1900+14 observed with the *XMM-Newton*EPIC-pn (upper data set in black) and the *Chandra*/ACIS in CC mode (lower data set in red). Solid lines are the best fitting STEMS model curves. Lower panel: residuals of the spectral fits.

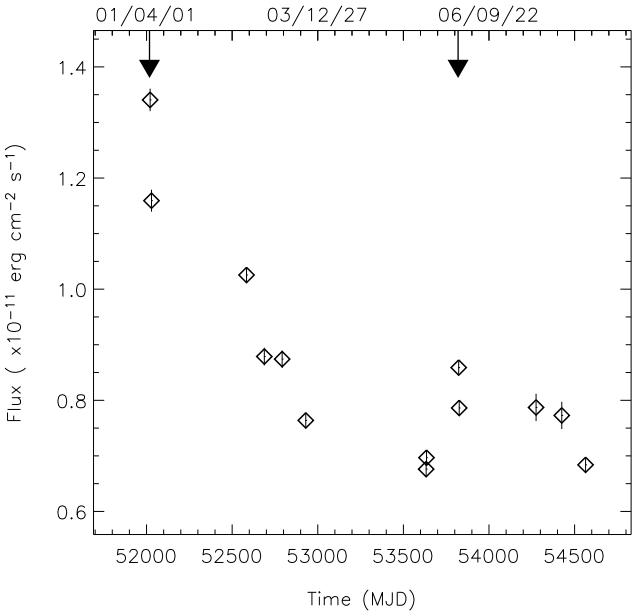

FIG. 2.— Unabsorbed flux history of SGR 1900+14 in the 0.8−6.5 keV range. The two arrows indicate the onset of the April 2001 and March 2006 reactivations of the source, respectively. The calendar dates on top of the figure are in the YY/MM/DD format.

combined fits. Note that errors reported throughout the paper are 1 σ.

We also investigated the potential effects of the cross calibration between the *Chandra*/ACIS in CC mode and the *XMM-Newton*/EPIC-pn on the determination of spectral parameters. To this end, we used two data sets, observation ID 7593 with *Chandra* and 0410580101 with *XMM-Newton* which were selected because they occurred at comparable source fluxes. We fit both spectra using STEMS as well as the empirical blackbody plus power law model, accounting for interstellar absorption in both cases. In this analysis, we again forced the absorption parameter to remain constant for both spectra as it is not observed to vary over time. In Figure 1, we present the two spectra along with the best fitting STEMS models. We found all parameters of both continuum models to be consistent between the *Chandra* and XMM spectra to within 1 σ errors. These results ensure that the use of two different instruments does not introduce any systematic biases in the joint spectral analysis.

We present in Figure 2 the history of the unabsorbed X-ray flux of SGR 1900+14 in the 0.8−6.5 keV band. The first *Chandra* observation took place four days after the intermediate event (Feroci et al. 2002). The source flux declined rapidly in the period soon after this event, dropping from $(1.34 \pm 0.02) \times 10^{-11}$ erg cm^{-2} s^{-1} to $(1.16 \pm 0.02) \times 10^{-11}$ erg cm^{-2} s^{-1} in only about six days. An even faster decline was seen in the contemporaneous *BeppoSAX* observations: the source flux in the 2−10 keV band was $(3.1 \pm 0.3) \times 10^{-11}$ erg cm^{-2} s^{-1} on 2001 April 18 and declined to $(1.06 \pm 0.04) \times 10^{-11}$ erg cm^{-2} s^{-1} in 11 days (Esposito et al. 2007). We observed a similar trend following the 2006 reactivation of the source as its flux drops from $(8.6 \pm 0.1) \times 10^{-12}$ erg cm^{-2} s^{-1} to $(7.9 \pm 0.1) \times 10^{-12}$ erg cm^{-2} s^{-1} in three days.

We further studied these long term persistent flux variations of SGR 1900+14 as follows: we determined the relative times of the first eight observations (which took place before 2006) with respect to the onset of the April 2001 outburst and those of the remaining five observations with respect to the onset of the March 2006 activation. We present in Figure 3 the unabsorbed flux as a function of relative time since each respective outburst onset. We found that in both outbursts the source flux declined rather gradually until about 600 days after the onset and exhibited a sharper decline trend beyond $\sim$ 600 days. We also found that SGR 1900+14 was at its lowest X-ray flux level of 6.8×10^{-12} erg cm^{-2} s^{-1} before the March 2006 reactivation. Following the source re-brightening after the 2006 outburst, the flux reached that level again in the last pointed observation.

To better understand the nature of these flux variations in SGR 1900+14, we investigated a possible correlation between the flux and the only varying STEMS parameter, i.e., the surface temperature. We find that the flux and surface temperature are indeed correlated, with a Spearman's rank order correlation coefficient $r = 0.72$. The probability of obtaining such a correlation with a random data set is $P = 0.005$. In Figure 4, we show the history of the surface temperature of the neutron star as well as its long term flux behavior. The decline in the surface temperature alone (assuming a single temperature) cannot account for the observed flux decline. In particular, the average surface temperature dropped from $\sim$ 0.56 keV to 0.53 keV as measured on 2001 April 22 (MJD 52021) and 2005 September 22 (MJD 53635), respectively, which corresponds to a flux decline of about 25% (if the emitting surface area remains constant). However, the source flux declined by about 97% between these two epochs, mostly soon after the rise; the remaining decline over the last 1100 days of the observing period was only about 33%, while the temperature decreased by about 6%.

We also investigated the long term behavior of the surface emitting area inferred using the STEMS normalization and surface temperature. We found that, for a

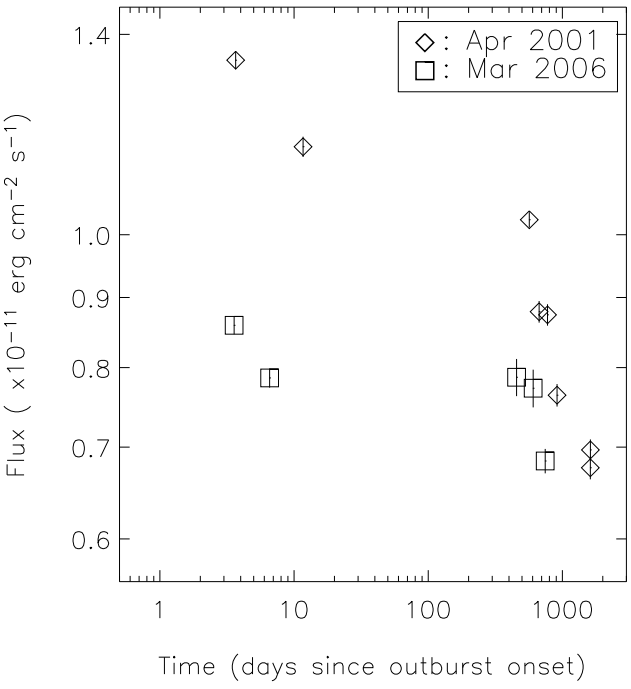

FIG. 3.— Unabsorbed flux of SGR 1900+14 in the $0.8-6.5$ keV range vs. relative time since the onset of the two bursting episodes: 2001 April (triangles) and 2006 March (squares).

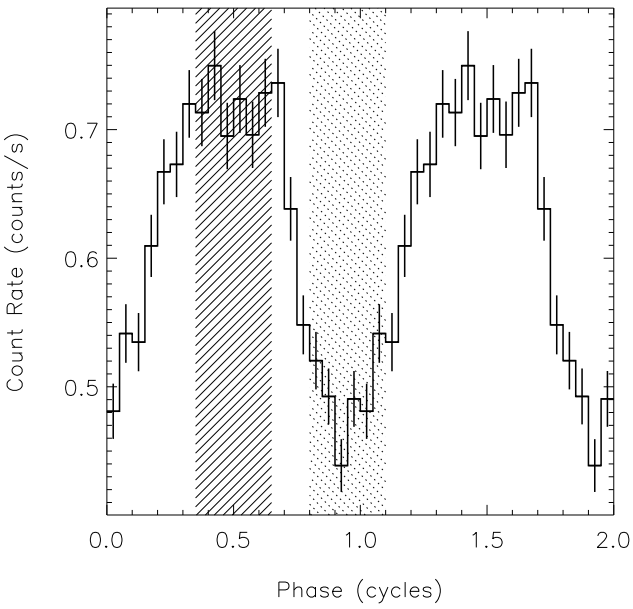

FIG. 5.— Pulse profile of SGR 1900+14 during the *Chandra* observations on 2001 April 22 (MJD 52021). The pulse phase intervals used as pulse peak and pulse minimum spectral accumulations are shown with hatched and dotted regions, respectively.

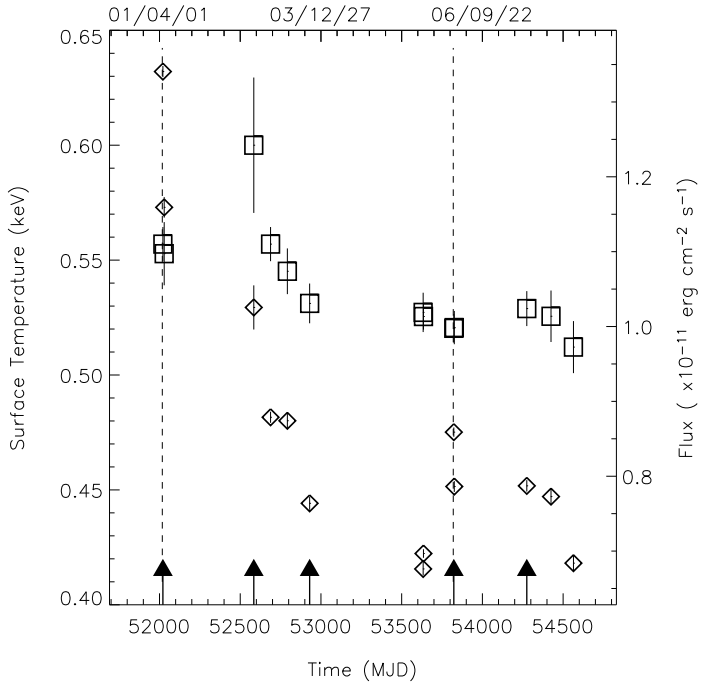

FIG. 4.— Evolution of the neutron star surface temperatures (squares) obtained by fitting each spectrum with STEMS, and the corresponding unabsorbed flux (diamonds). The vertical dashed lines indicate the onsets of the 2001 and 2006 outbursts, respectively. Arrows at the lower end of the figure indicate observations used in further phase resolved spectral analysis (see the text). Calendar dates on top are in the YY/MM/DD format.

uniform surface temperature, the radius of the emitting region is 4.8±0.2 km soon after the 2001 outburst onset (assuming a distance to SGR 1900+14 of 13.5 kpc; Vrba et al. 2000). It then declined to 3.9±0.2 km and remained fairly constant until 2005. The radius emitting surface went up again to 4.4±0.1 km following the 2006 outburst but quickly fell to a marginally higher constant level of 4.1±0.2 km. This change, however, could be the result of neglecting temperature inhomogeneities. Note also that the errors in the surface temperature and normalization, and, consequently, in the radius of the emitting area, are correlated.

Finally, we performed a coarse phase resolved spectral analysis using five *Chandra* observations (indicated by arrows in Figure 4) to check whether there are significant surface temperature variations over the spin phase, which may affect or bias the spectral determination of the phase-averaged temperature. For each of the selected pointings, we obtained a pulse peak spectrum (spanning 0.30 of the spin phase during the pulse peak) and a pulse minimum spectrum (spanning 0.30 of the spin phase during the pulse minimum) using accurate and contemporaneous pulse period reported in Mereghetti et al. (2006). We show in Figure 5 the pulse profile and pulse phase intervals within which the pulse peak and pulse minimum spectra were obtained in the observation on 2001 April 22 (MJD 52021). We fit the X-ray spectra in the 0.8−6.5 keV using STEMS with surface magnetic field strength and magnetospheric parameters fixed at their phase averaged values. In Table 2, we list the temperatures and model normalizations (i.e., an indicator of intensity) for the five selected observations. We find that the surface temperature remains constant over the spin phase of the source in the majority of these observations.

TABLE 2
Spectral Fit Results of the Phase-resolved Analysis

Obs Date (MJD)	Pulse Peak Temperature (keV)	Pulse Minimum Temperature (keV)	Peak Normalization (10^{-10})	Min Normalization (10^{-10})
52021	0.57±0.01	0.54±0.01	2.2±0.3	1.8±0.1
52584	0.56±0.01	0.55±0.01	1.6±0.1	1.2±0.1
52930	0.53±0.01	0.52±0.01	0.57±0.05	0.48±0.05
53823	0.53±0.01	0.52±0.01	0.26±0.03	0.19±0.02
54275	0.55±0.01	0.47±0.01	0.37±0.03	0.5±0.2

4. DISCUSSION

We found that SGR 1900+14 exhibits a monotonic but non-steady flux decline following the X-ray brightening during its 2001 and 2006 outbursts. In both outbursts, its flux dropped rapidly within a few weeks after the onset of the outburst and then at a slower rate for approximately 600 days. After this period, the flux declines again at a much faster rate. A similar decay trend was also seen in SGR 1627−41 (Kouveliotou et al. 2003). The fact that we observe the same trend in successive outbursts from the same source suggests that the long-term effects of outbursts are not stochastic but reproducible.

It is clear that magnetar bursting activity leads to long-term flux enhancements and that the additional energy powering these enhancements is stored in the crust as heat. This heat comes most likely from the energy released in the crust during the bursts, or from the energy deposited in the crust by the bombardment with magnetospheric particles during the burst. The crust, then, reradiates this additional heat over a timescale of a few years.

Despite the correlation between the flux and the surface temperature, the variation in the surface temperature alone does not account for the decline in the flux, but it also requires a change in the emitting area over time. This can perhaps be understood if the crust is heated inhomogeneously, as would be expected if the initial heating episode is due to magnetic energy release. Moreover, because the thermal resistance of the crust is dominated by the uppermost layers, where the heat conductivity is strongly affected by the magnetic field, heat coming from the deeper layers of the crust could reach the surface unevenly. This leads to both uneven heating and uneven cooling, which may affect the total inferred emitting area. Furthermore, over-time, because the observations are carried out in a limited energy range, cooler parts of the crust may fall out of the observed energy band faster than the hotter regions, again reducing the inferred emitting area. Thus, the observed source flux would decline both due to a decline in temperature as $\propto T^4$ and due to a decline in the emitting area.

We find on three different occasions that the X-ray flux of SGR 1900+14 was as low as 6.8×10^{-12} erg cm^{-2} s^{-1}, suggesting that this level may correspond to the source persistent X-ray flux in the absence of burst induced enhancements. The current detection thresholds of imaging instruments are $\sim 10^{-13}$ erg cm^{-2} s^{-1}; it is, therefore, possible that the persistent flux levels of the so-called transient magnetars are much lower than those of the always detectable magnetars. If that is indeed the case, the magnetar engine that is responsible for a source persistent quiescent X-ray emission would seem to power a broad flux range of $\lesssim 10^{-13}$ to $\sim 10^{-10}$ erg cm^{-2} s^{-1}.

E.G., T.G., and F.Ö. acknowledge EU FP6 Transfer of Knowledge Project Astrophysics of Neutron Stars (MTKD-CT-2006-042722). D.E. acknowledges support from the Israel Science Foundation, the U.S. Israel Binational Science Foundation, and the Joan and Robert Arnow Chair of Theoretical Astrophysics.

REFERENCES

Anders, E., & Grevesse, N. 1989, GeCoA, 53, 197
Arnaud, K. A., 1996, in Astronomical Data Analysis Software and Systems V, eds. Jacoby G. and Barnes J., p17, ASP Conf. Series Vol. 101
Dib, R., Kaspi, V.M., & Gavriil, F.P., 2009, ApJ, 702, 614
Duncan, R. C., & Thompson, C. 1992, ApJ, 392, L9
Esposito, P., et al. 2007, A&A, 461, 605
Feroci, M. et al. 2002, in Neutron Stars in Supernova Remnants, eds. P. O. Slane and B. M. Gaensler, ASP Conference Series, Vol. 271, 285
Göğüş, E. et al. 2010, ApJ, 718, 331
Guidorzi, C., et al. 2001, GCN Circ., 1041, 1
Güver, T., Özel, F., Göğüş, E., & Kouveliotou, C. 1999, ApJ, 667, L73
Güver, T., Özel, F., & Lyutikov, M. 2006, ApJ, submitted (arXiv:astro-ph/0611405)
Halpern, J. P. & Gotthelf, E. V. 2005, ApJ, 618, 874
Hurley, K., et al. 1999, ApJ, 510, L111
Israel, G. L., et al. 2007, ApJ, 664, 448
Kouveliotou, C., et al. 1993, Nature, 362, 728
Kouveliotou, C., et al. 1999, ApJ, 510, L115
Kouveliotou, C., et al. 2001, ApJ, 558, L47
Kouveliotou, C., et al. 2003, ApJ, 596, L79
Lyutikov, M. & Gavriil, F. 2006, MNRAS, 368, 690
Mazets, E. P., Golenetskij, S. V. & Guryan, Y. A. 1979, Soviet Astronomy Letters, 5, 343
Mereghetti, S. 2008, Astron Astrophys Rev, 15, 225
Mereghetti, S. et al. 2006, ApJ, 653, 1423
Ng, C. -Y., et al. 2010, ApJ, in press (arXiv:1008.1165)
Özel, F. 2001, ApJ, 563, 276
Özel, F. 2003, ApJ, 583, 402
Özel, F. & Güver, T. 2007, ApJ, 659, L141
Thompson, C., & Duncan, R. C. 1996, ApJ, 473, 322
Thompson, C., Lyutikov, M., & Kulkarni, S. R. 2002, ApJ, 574, 332
Vetere, L., et al. 2006, GCN 4922, 1
Vrba, F. et al., 2000, ApJ, 533, L17
Woods, P. M., et al. 2001, ApJ, 552, 748
Woods, P. M., et al. 2004, ApJ, 605, 378
Woods, P.M., & Thompson, C. 2006, in Compact Stellar X-ray Sources, eds. W.H.G. Lewin & M. van der Klis, Cambridge Astrophysics Series, 39, p.547